Flow (2023), **3** E25
doi:10.1017/flo.2023.15

FLOW CAMBRIDGE UNIVERSITY PRESS

RESEARCH ARTICLE

Stream lamination and rapid mixing in a microfluidic jet for X-ray spectroscopy studies

Diego A. Huyke[1,‡], Alexandre S. Avaro[1,‡], Thomas Kroll[2] and Juan G. Santiago[1,*]

[1]Department of Mechanical Engineering, Stanford University, Stanford, CA 94305, USA
[2]Stanford Synchrotron Radiation Lightsource, SLAC National Accelerator Laboratory, Stanford University, Menlo Park, CA 94025, USA
*Corresponding author. E-mail: juan.santiago@stanford.edu
‡Equal contribution.

Received: 27 February 2023; **Revised:** 23 May 2023; **Accepted:** 1 June 2023

Keywords: Laminar mixing; Microfluidics; Jets; Flow focusing; Reacting microflow; X-ray spectroscopy

Abstract

Microfluidic mixers offer new possibilities for the study of fast reaction kinetics down to the microsecond time scale, and methods such as soft X-ray absorption spectroscopy are powerful analysis techniques. These systems impose challenging constraints on mixing time scales, sample volume, detection region size and component materials. The current work presents a novel micromixer and jet device which aims to address these limitations. The system uses a so-called 'theta' mixer consisting of two sintered and fused glass capillaries. Sample and carrier fluids are injected separately into the inlets of the adjacent capillaries. At the downstream end, the two streams exit two micron-scale adjoining nozzles and form a single free-standing jet. The flow-rate difference between the two streams results in the rapid acceleration and lamination of the sample stream. This creates a small transverse dimension and induces diffusive mixing of the sample and carrier stream solutions within a time scale of 0.9 microseconds. The reaction occurs at or very near a free surface so that reactants and products are more directly accessible to interrogation using soft X-ray. We use a simple diffusion model and quantitative measurements of fluorescence quenching (of fluorescein with potassium iodide) to characterize the mixing dynamics across flow-rate ratios.

Impact Statement

This study presents the design, demonstration and quantification of a novel mixer designed to address constraints associated with reaction rate studies using soft X-ray spectroscopy. Low-flow-rate, rapid micromixers typically use laminar flow focusing where a sample stream is confined within a carrier stream and, often, within a microfluidic device. This limits the possible spectroscopic methods to hard X-ray spectroscopy, including significant absorption by the carrier stream and microfluidic device, and reduced energy resolution. In this study, the sample is laminated at the surface of a free jet to allow direct optical access to the mixing zone. We demonstrate and quantify a mixing time scale of 0.9 μs. The mixing and reaction occur within approximately 0.1 μm from the surface of the jet. This micromixer thus enables the analysis of reactions with fast kinetics using techniques with demanding experimental constraints such as the 3d transition metal L-edge X-ray absorption spectroscopy (XAS).

1. Introduction

Interest in time-resolved studies of structural biology continues to grow (Brändén & Neutze, 2021). X-ray methods which incorporate microfluidic mix-and-inject devices enable the study of processes triggered by chemical potentials (e.g. protein folding) (Pollack et al., 1999). In large part because of the line-of-sight integrating nature of X-ray methods, the mixing function of these microfluidic devices has been achieved using three-dimensional (3-D) hydrodynamic focusing (Huyke et al., 2020, 2021; Plumridge et al., 2018). Furthermore, the sample injection task is increasingly achieved using microfluidic devices that produce free jets to accommodate the highly powerful radiation of next-generation X-ray sources (Crissman et al., 2022; Ishigami et al., 2019; Knoška et al., 2020; Wang, Weierstall, Pollack, & Spence, 2014). While 3-D focusing can enable rapid mixing (order microseconds) and free-jet delivery avoids X-ray interactions with device materials, the integration of 3-D focusing and subsequent jetting results in a sample stream surrounded by an annular liquid jet.

A microfluidic, gas-accelerated jet with a 3-D hydrodynamically focused stream was first demonstrated by Gañán-Calvo (1998). Later, mixing coupled with jet delivery was first demonstrated for X-ray detection by Wang et al. (2014). The latter work used three coaxial capillaries, first to focus a fluorescein sample stream with a potassium iodide (KI)-containing carrier stream and then to accelerate the stream into a jet (DePonte et al., 2008). The system by Wang et al. reported a 250 μs mixing time and jet diameter of 3 to 7 μm. Olmos et al. modified the previous construction by including a smaller diameter 'delay region' downstream of the initial sample–sheath interaction region (Olmos et al., 2018). This delay region allowed for mixing in as short as 5 ms. Recently, Knoška et al. developed a 3-D-printed mix-and-inject device based on chaotic refolding and subsequent gas acceleration (Knoška et al., 2020). However, KI mixing experiments therein resulted in an estimated mixing time of 100 ms.

We here introduce a novel, jet-based mix-and-inject device which initiates mixing and jetting simultaneously. To accomplish this, we use commercially available, so-called theta capillaries. Theta capillaries result from fusing two glass capillaries at one end and pulling these at elevated temperature. In our scheme, a thin sample stream is laminated above a thick carrier stream just downstream of the theta-shaped, dual-outlet nozzle of the system. This enables fast mixing and windowless detection of sample molecules at the surface of the jet. An order 10 μl min^{-1} stream is used for sample and a second, order 1 ml min^{-1} stream is used as a carrier fluid. The latter stream enables a stable, free jet with a length of over 2 mm. The device is designed to reduce experimental background signal associated with X-ray absorption by the solvent or reactant molecules of the carrier fluid stream. A secondary advantage of the lack of an outer (i.e. surrounding) sheath and hence direct access to the (mixed) sample stream is the possibility to perform fluorescence yield L-edge XAS on e.g. 3d transition metal complexes. The latter can be used to achieve ~3 times higher resolution spectra as compared with the Fe K-edge XAS data described earlier for a hydrodynamic focusing mixer (Huyke et al., 2021). The main advantage of this mixer configuration is therefore to enable direct access by the X-ray beam to the reactants and products carried by the liquid stream within approximately 100 nm of the free surface of the jet. The latter dimension is, for example, of the order of the photon absorption and escape length for XAS applications (Henke, Gullikson, & Davis, 1993). We here first discuss the design, operation and experimental fabrication of our device. We then present experimental results of fluorescein quenching experiments which reveal a mixing time of the order of microseconds. We also present a simple, one-dimensional (1-D) diffusion model to inform the scaling of spatio-temporal data and to analyse the mixing time scale.

2. Device design and set-up

This section introduces the so-called theta device design, operating principle and experimental set-up. The device and experimental set-up are described in figure 1. The device is designed to provide rapid mixing at (and very near) the surface of a free jet. To achieve this, we used a commercially available theta capillary (TG150-4, Warner Instruments, USA). This system is fabricated from two independent glass capillaries. The upstream portion of these capillaries are two separate, parallel capillary inlets with

https://doi.org/10.1017/flo.2023.15 Published online by Cambridge University Press

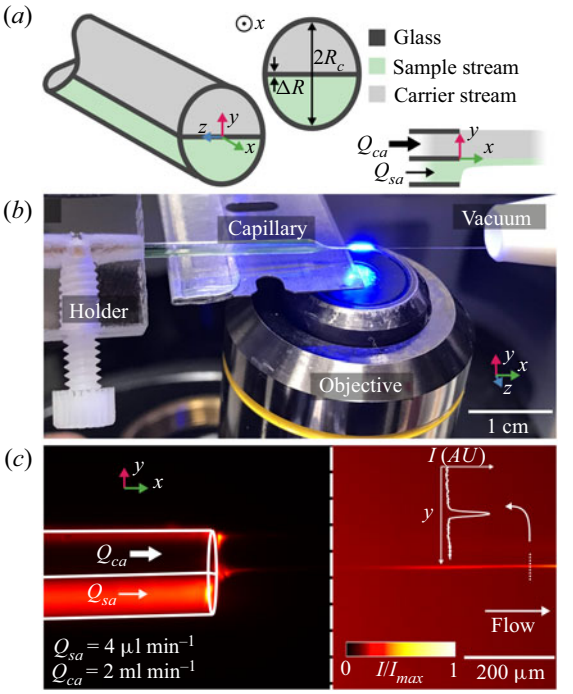

Figure 1. *Device schematic and experimental set-up. (a) Theta mixer schematic in isometric, front and side views. (b) Image of experimental set-up during operation with the jet exiting into the atmosphere just above the microscope objective. A vacuum line was used to receive the free jet. A razor blade blocked illumination of the jet nozzle tip. (c) Experimental epifluorescence image of the device's dual-nozzle during operation. The image to the left of the vertical dashed line was taken without the razor blade in place. The image to the right shows the downstream jet (with razor blade). The inset plot shows a profile of measured jet fluorescence intensity at the location of the dotted line.*

initial radii of 0.5 mm. They are sintered together (by the manufacturer) over a portion of their length so that the flow through the device exits from two fused and adjoining nozzles. We further shaped the outlet portion of these systems by heating and pulling using a laser-based micropipette puller (P-2000, Sutter Instrument, USA). In this way, we created a series of flow systems with outlet nozzles with characteristic radii R_c varying between 10 and 100 μm. As indicated in the schematic of figure 1(*a*) and the side-view image of figure 1(*c*), each of the two outlet nozzles has a semicircular shape. For the experimental studies described here, we used devices with 100 and 15 μm radii, as indicated in figures 1 and 3. The device and laser-based puller are described further in supplementary material figures S1 and S2 available at https://doi.org/10.1017/flo.2023.15.

To create a lamination mixer and jet, a high-flow-rate 'carrier' stream Q_{ca} is injected into one of the capillary inlets. Through the second inlet, we introduce a sample stream with a flow rate Q_{sa} that is approximately 20 to 100 times lower than Q_{ca}. The two liquid streams come into contact near the outlet of the nozzle and form a single, free-standing jet. The larger-flow-rate stream is used to achieve a contiguous jet prior to Rayleigh–Plateau-type breakup (Middleman, 1965). The contiguous jet extends a few millimetres from the nozzle. The low-flow-rate sample stream is quickly accelerated and laminated resulting in a small time scale for the transverse diffusion of reactant species. This achieves well-controlled and rapid mixing at and near the surface of a free, liquid jet.

The flow device (figure 1*b*) was mounted on a custom capillary holder (THP-15, Warner Instruments, USA) and oriented such that the jet emerged horizontally over the objective of an inverted epifluorescence microscope (IX70, Olympus, USA) used to image the jet. We used objectives with 4× magnification

https://doi.org/10.1017/flo.2023.15 Published online by Cambridge University Press

(numerical aperture, NA = 0.2) (PlanApo, Nikon, Japan) and 10× magnification (NA = 0.4) (UPlanApo, Olympus, Japan). Images were acquired with an sCMOS camera (ORCA-Flash4.0 V2, Hamamatsu, Japan). Aqueous solutions were pumped into the device using high performance liquid chromatography (HPLC) pumps (LC-20AD, Shimadzu, Japan). All jets exited into atmospheric pressure. Downstream of the jet, a barbed nozzle connected to a vacuum source collected the jet liquid. The experimental set-up including supply lines and connections is described further in supplementary material § S2.

Standard illumination of the entire field of view (including nozzle tip) resulted in strong elastic scatter from the nozzle tip, and this optical scatter tended to saturate measured image intensities. To prevent this (and better image the resulting jet), we used a razor blade to partially block the illumination, as shown in the figure. The images of our jet (e.g. as we shall discuss in figure 3) therefore cropped out the first roughly 25 μm of the jet development region just downstream of the device aperture.

For visualization, a buffered solution with 50 μM fluorescein was injected into the sample channel (figure 1*c*) and the same buffer (without fluorescein) was injected into the other channel. All solutions were buffered with 20 mM Tris and 10 mM HCl (measured pH = 8). Experimental images showed that a thin stream of sample solution was laminated on one side of the jet (cf. figure 1).

3. Results and discussion

We first describe a simple diffusion model used to scale experimental data and then present our experimental study of mixing kinetics. For the latter, we use fluorescein quenching to quantify the degree and rate of mixing. Quenching was achieved by injecting buffered fluorescein and buffered 500 mM KI, respectively, into the sample and carrier channels.

3.1. One-dimensional diffusion and quenching model

In this section, we present a simple analysis of the mixing and fluorescence quenching process which is useful in scaling experimental data and estimating mixing rates. All of our experiments were performed under Eulerian steady state flow conditions. As we shall discuss, this results in profiles of line-of-sight-integrated fluorescence intensity versus downstream location along the jet. We compare these profiles for the cases of quenching and no quenching to deduce the degree and rate of mixing.

As a simple model, we will assume that the observable jet quickly develops such that the liquid velocity U_j is approximately uniform along the cross-section and along the streamwise direction. This lets us assume a simple relation between the downstream location and the time over which the two streams can diffuse and mix. This spatio-temporal relation can be expressed as $x \approx U_j t$, where x is the streamwise coordinate just downstream of the nozzle tip (at the start of the field of view) and U_j is the developed jet velocity.

The axial diffusive flux in this system is much slower than that of axial advection. For example, the streamwise Péclet number of the form $R_c U_j / D_{sa}$ is order 10^6 or greater, where D_{sa} is the diffusion coefficient of the sample in water. Hence, we will consider an analogous problem of unidimensional unsteady diffusion of the two streams. In this unsteady model, time is a simply a surrogate for the streamwise coordinate x as per the spatio-temporal relation above. This simple model neglects the initial complex 3-D development of the jet (particularly near the nozzle exits). We will use this model to inform our choice of scaling parameters to describe the observed rates of mixing.

We consider the 1-D diffusion of the sample species and quencher species across the jet. As such, we model the steady jet as two layers of fluid, as shown in figure 2(*a*). Here, we note by x the streamwise direction and ξ the transverse direction (parallel to the y coordinate in figure 1). The origin of ξ is the (top) free surface of the sample region of the jet and ξ is oriented into the jet. The jet domain is represented by $x > 0$ and $\xi > 0$. The top, laminated sample layer has transverse thickness s and the bottom carrier layer has some thickness $2R_j \gg s$. As we shall discuss further below, the initial dimension s is a constant related to the flow rate of the sample stream. In the physical problem, the jet fluid moves at a uniform,

https://doi.org/10.1017/flo.2023.15 Published online by Cambridge University Press

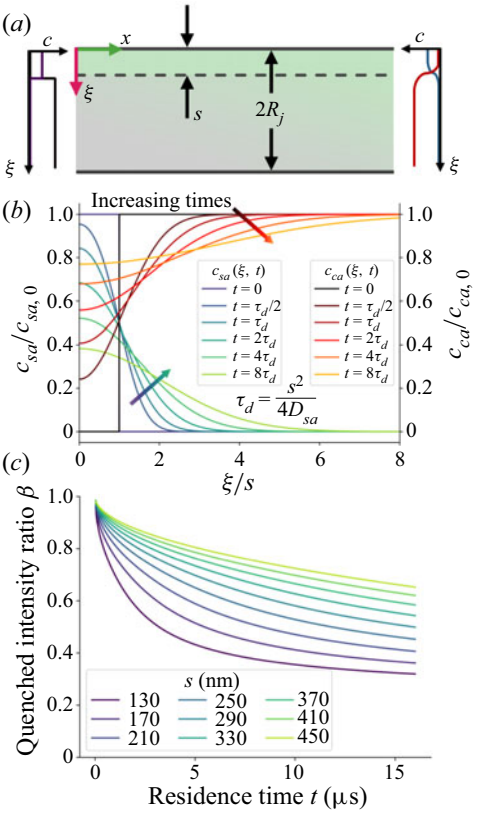

Figure 2. *One-dimensional diffusion model for the theta device. (a) The jet is modelled by two superposed 1-D layers. The top layer* $(0 < \xi < s)$ *has initially concentration* $c_{sa,0}$ *of sample and no inhibiter while the bottom layer* $(s < \xi < 2R_j)$ *has concentration* $c_{ca,0}$ *of quencher and no sample. The fluid moves from left to right at velocity* U_j *such that* $x = U_j t$*. (b) Concentration profiles for sample (left) and quencher (right) at six time instants. These profiles are given by (3.5) and (3.6). (c) Numerical solution for* $\beta(t, s)$ *for various values of the initial transverse thickness s. These profiles are obtained by numerically integrating equation (3.9).*

steady Eulerian velocity U_j in the x direction. In the analogous unsteady diffusion problem, we define $t = 0$ as the time (near the nozzle exits) when the two streams first begin to diffuse together and mix. Using these assumptions, the 3-D steady advection–diffusion problem is roughly approximated using the following unsteady 1-D diffusion problem:

$$\frac{\partial c_{sa}}{\partial t} = D_{sa}\frac{\partial^2 c_{sa}}{\partial \xi^2}, \tag{3.1}$$

$$\frac{\partial c_{ca}}{\partial t} = D_{ca}\frac{\partial^2 c_{ca}}{\partial \xi^2}, \tag{3.2}$$

$$c_{sa}(t = 0, \xi) = c_{sa,0}(1 - \mathcal{H}(\xi - s)), \tag{3.3}$$

$$c_{ca}(t = 0, \xi) = c_{ca,0}\mathcal{H}(\xi - s). \tag{3.4}$$

Here, c_{sa}, $c_{sa,0}$, c_{ca} and $c_{ca,0}$ are respectively the concentration of sample (in our case, fluorescein) in the jet, initial concentration of sample species in the sample stream, quencher (here, KI) concentration in the jet and the initial quencher concentration in the carrier stream, D_{sa} and D_{ca} are, respectively, the

https://doi.org/10.1017/flo.2023.15 Published online by Cambridge University Press

diffusion coefficients of sample and inhibiter in water, $\mathcal{H}$ is the Heaviside function and s is the 1-D transverse thickness of the thin laminated sample stream on top of the free jet.

The solution of the 1-D problem is the following:

$$c_{sa}(\xi, t) = \frac{c_{sa,0}}{2}\left[\mathrm{erf}\left(\frac{\xi + s}{\sqrt{4D_{sa}t}}\right) - \mathrm{erf}\left(\frac{\xi - s}{\sqrt{4D_{sa}t}}\right)\right], \tag{3.5}$$

$$c_{ca}(\xi, t) = \frac{c_{ca,0}}{2}\left[2 + \mathrm{erf}\left(\frac{\xi - s}{\sqrt{4D_{ca}t}}\right) - \mathrm{erf}\left(\frac{\xi + s}{\sqrt{4D_{ca}t}}\right)\right]. \tag{3.6}$$

Figure 2(b) shows successive solutions for c_{sa} and c_{ca} at various times. We present a derivation of this solution in supplementary material § S3.

The measured signal is a function of the volume-integrated number of fluorescent molecules and the degree of quenching. We therefore compare the signal in the presence versus absence of the inhibiter species. In the absence of quencher, the measured image intensity is proportional to line-of-sight-integrations of fluorescence as follows:

$$I_{unquen}(x, y, t) \propto \int_0^{2R_j} c_{sa}(\xi, t)\,\mathrm{d}\xi\ . \tag{3.7}$$

Here, the subscript 'unquen' refers to the integrated image intensity captured at the image plane of the camera. The dependence on coordinates x and y represents the variations along the image plane. In the presence of the quencher, the measured image intensity is governed by the Stern–Volmer relation as follows:

$$I_{quen}(x, y, t) \propto \int_0^{2R_j} \frac{c_{sa}(\xi, t)}{1 + K_{sv}c_{ca}(\xi, t)}\,\mathrm{d}\xi. \tag{3.8}$$

Here, 'quen' indicates the quenched case and K_{sv} is the Stern–Volmer constant ($K_{sv} = 7.29\ \mathrm{M}^{-1}$ for iodide quenching fluorescein; Huyke et al., 2020). Therefore, the quenched-to-unquenched ratio β is given by

$$\beta(x, y, t; s) = \frac{I_{quen}}{I_{unquen}} = \frac{\int_0^{2R_j} \frac{c_{sa}(\xi,t)}{1+K_{sv}c_{ca}(\xi,t)}\,\mathrm{d}\xi}{\int_0^{2R_j} c_{sa}(\xi, t)\,\mathrm{d}\xi}. \tag{3.9}$$

We know of no analytical closed-form solution for β for the distributions given by (3.5) and (3.6). We show in figure 2(c) the time evolution of β for various values of s based on numerical integration for $\int_0^{2R_j} (c_{sa}(\xi, t)/(1 + K_{sv}c_{ca}(\xi, t)))\,\mathrm{d}\xi$.

We provide in the supplementary material an analytical approximation of the quantity β. In our regime, β is well approximated by

$$\begin{aligned}\beta(t; s) \cong\ & \frac{\frac{\sqrt{4D_{sa}t}}{s}\mathrm{erf}\left(\frac{s}{\sqrt{4D_{sa}t}}\right)\left(1 - \frac{D_{sa}}{D_{ca}}\right)}{1 + K_{sv}c_{ca,0}\left(1 - \mathrm{erf}\left(\frac{s}{\sqrt{4D_{ca}t}}\right)\right)} \\ & \times \left(1 + \mathrm{e}^{(1-s/\sqrt{4D_{sa}t})/(1-D_{sa}/D_{ca})}\right)\ln\left(1 + \mathrm{e}^{(s/\sqrt{4D_{sa}t}-1)/(1-D_{sa}/D_{ca})}\right).\end{aligned} \tag{3.10}$$

We provide in supplementary material § S4 of the SI a comparison of the approximate solution (3.10) with the numerically integrated solution from (3.9) (cf. figures S4c and S4d). The quenched intensity ratio β depends on the initial transverse thickness of the sample stream s, the diffusivity ratio D_{sa}/D_{ca} and the (non-dimensional) product $K_{sv}c_{ca,0}$. Time appears only in terms of the form $s/\sqrt{4Dt}$, which suggests a characteristic time scale of $\tau = s^2/D$. We shall use this as an approximate time scale of the observed, line-of-sight-averaged quenching dynamics in the jet. This scaling will also inform our

https://doi.org/10.1017/flo.2023.15 Published online by Cambridge University Press

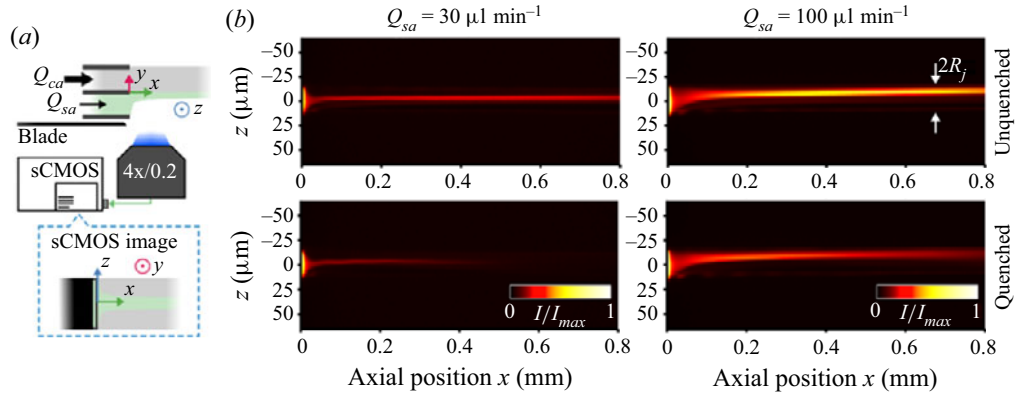

Figure 3. *Example experimental data for mixing using quenched fluorescence visualization. (a) Schematic of the imaging set-up for quenching experiments. The inset and coordinate systems inform the orientation of the images on the right. (b) Experimental images of fluorescein under unquenched (top row) and quenched (bottom row) reaction conditions. Representative data are shown for sample flow rates, Q_{sa}, of 30 (left column) and 100 µl min^{-1} (right column) while the carrier flow rate Q_{sa} was fixed at 2 ml min^{-1}.*

estimate of the mixing time scale from measurements of the spatial distribution of the fluorescence intensity as a function of sample flow rate.

3.2. Visualization and mixing quantification experiments

We now present experimental quantification of mixing and fluorescence quenching using the theta device. Figure 3 shows a schematic and representative jet images for experiments where we varied Q_{sa} and maintained a fixed Q_{ca} = 2 ml min^{-1}, with and without KI in the carrier stream. Figure 3(*a*) shows a schematic of the imaging set-up (top) and the image captured by the camera (bottom). Epifluorescence images of the jet were acquired in the streamwise–spanwise plane, such that the excitation light passed through the microscope objective and illuminated the laminated sample stream without traversing the carrier stream. Light in the emission wavelength range was captured by the objective. Figure 3(*b*) shows examples images for two sample stream flow rates, with (top) and without (bottom) quencher solute in the carrier stream. The unquenched images (top row) show that the sample width (along the z-direction) decreases with the sample flow rate Q_{sa}. We attribute this rapid variation to the 3-D initial development of the jet as the streams exit the nozzles and adjoin. Importantly, the quenched images (bottom row) comparatively show strong quenching of fluorescein within 0.8 mm along the axial direction x. The lower Q_{sa} condition shows the sample stream fluorescence is nearly completely quenched at $x = 0.6$ mm.

We quantified the degree of quenching by computing the quenched intensity ratio, β, as a function of spatial location along the jet (Huyke et al., 2021). Briefly, we integrated the quenched and unquenched pixel intensities along the spanwise z-direction, obtained the ratio of these (streamwise) distributions and plotted this ratio as a function of the streamwise coordinate, x. The quenched intensity ratio was observed for Q_{sa} between 20 and 100 µl min^{-1} and fixed Q_{ca} = 2 ml min^{-1} (figure 4*a*). As an approximate sample residence time t_{appr}, we estimated the jet velocity U_j as $(Q_{ca} + Q_{sa})/A_j$ where A_j is the cross-sectional area of the free jet. Note that the cross-sectional area of a jet is expected to be substantially smaller than the exit areas of the nozzles as the jet develops and accelerates (Haustein, Harnik, & Rohlfs, 2017). We present in supplementary material § S5 of the SI a derivation for the estimation of the free-jet cross-sectional area $A_j = \pi R_j^2$ and exit velocity U_j. We consider the control volume shown in figure S5(*d*). At the inlet, we assume the fully developed velocity profile of both semi-circular channels as specified in (S22a) and (S22b) (White, 2006). At the outlet, we assume the two streams have merged into a single

https://doi.org/10.1017/flo.2023.15 Published online by Cambridge University Press

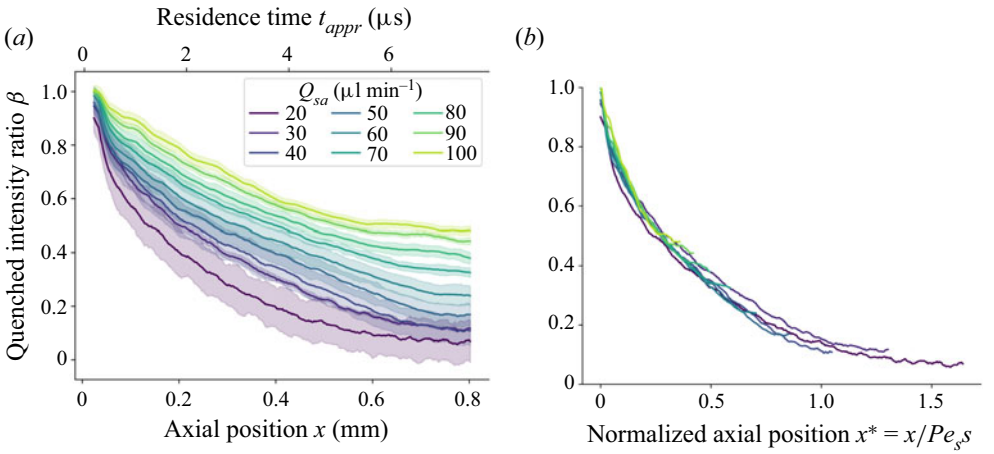

Figure 4. *Measured quenched-to-unquenched fluorescence intensity ratios, β. These are quenched-to-unquenched intensity ratios of the z-direction-integrated image intensities as a function of axial position. (a) Quenched intensity ratio β versus axial position x (bottom abscissa) and estimated sample residence time (top abscissa) for nine values of Q_{sa} and fixed $Q_{ca} = 2$ ml min^{-1}. Note the estimated sample residence time does not account for the 3-D rapid jet development upon exiting the theta capillary. Shaded areas indicate regions of uncertainty as $\beta \pm P_\beta$, where P_β indicates confidence on the mean. P_β is quantified in detail in supplementary material § S6. (b) Quenched intensity ratio versus non-dimensional position $x^* = (1/Pe_s)(x/s)$ (bottom abscissa) for the same nine values of Q_{sa} and fixed Q_{sa}. Here, s is derived from the 1-D diffusion model developed in § 3.1.*

free jet with a circular cross-section. We conserve mass and momentum flux over this control volume and derive the following expression for U_j and R_j:

$$U_j = \frac{1}{R_c^2}\frac{Q_{sa}^2 + Q_{ca}^2}{Q_{sa} + Q_{ca}}\left(\frac{2\pi}{8-\pi^2}\right)^2\left(\frac{184}{27\pi} - \frac{\pi}{6} - \frac{64}{9\pi}\ln(2)\right), \tag{3.11}$$

$$R_j = R_c\frac{Q_{sa} + Q_{ca}}{\sqrt{Q_{sa}^2 + Q_{ca}^2}}\frac{\pi^2 - 8}{2\pi\sqrt{\frac{184}{27} - \frac{\pi^2}{6} - \frac{64}{9}\ln(2)}}. \tag{3.12}$$

Here, R_c is the radius of the theta device, as shown in figure 1(*a*).

The quenched intensity ratio, as expected, is near unity at the $x = 0$ position (defined at the start of the field of view just downstream of the nozzle exit). This ratio rapidly decreases along the x direction. Decrease of Q_{sa} (for a fixed Q_{ca}) results in more rapid diffusion and quenching, and we attribute this to a decrease of the characteristic distance of mixing (analogous to the parameter s in the simple 1-D model). The characteristic mixing time is here characterized in terms of the Lagrangian time experienced by a fluid particle traveling with the jet at Eulerian velocity U_j. This Lagrangian time is shown as the top abscissa in figure 4(*a*). The time to reach 50 % of the maximum quenching varied between approximately 0.9 to 5 μs for Q_{ca}/Q_{sa} ratios of 100 and 20, respectively. The jet velocity U_j is approximately 125 m s^{-1} for all experiments, and the observed length of the stable jet was more than 2 mm prior to Rayleigh–Plateau-type breakup.

Next, we explore the scaling of the data shown in figure 4(*a*) using the characteristic mixing time scale suggested by the simple model of § 3.1. To this end, we relate the s dimension of the 1-D model to the characteristic radial thickness of the actual sample stream. This process is described in more detail in supplementary material § S5 of the SI, and we summarize it here. Briefly, we approximate the shape of the free jet as a circular cross-section comprising two adjacent circular segments. Each segment

https://doi.org/10.1017/flo.2023.15 Published online by Cambridge University Press

originates from one nozzle exiting the theta capillary, as shown in figure S5(*c*). We assume that the chord length w of this circular segment is equal to the in-plane width of the sample stream, which we measure using epifluorescence images such as the one shown in figure 3(*b*). We relate w to the sagitta of the sample stream circular segment s' the simple geometric relation between chord and sagitta (cf. (S45)); s' serves as a first estimate of the sample stream transverse thickness. Of course, the simple model derived in § 3.1 does not capture the highly 3-D convection–diffusion effects of the physical problem. To account for this, we developed a simple heuristic to relate s' to the effective transverse thickness s of the sample stream, applicable to the 1-D diffusion model. To this end, we assume a proportional relation of the form $s = \lambda s'$. Here, λ is a single empirical constant of proportionality (i.e. across all values of the sample flow rate) determined by the fit of the quenched intensity ratio β from the experimental data shown in figure 4(*a*) to the model developed in § 3.1. This approximation yields $\lambda \approx 0.2$. We show the resulting scaling in figure 4(*b*) in which the axial position x is normalized by a characteristic length of the form $s\,Pe_s$. Here, $Pe_s = sU_j/D_{ca}$ is a Péclet number based on the estimated transverse sample stream transverse thickness s and D_{ca}, the diffusivity of the carrier liquid. The value of D_{ca} is approximately three times greater than D_{sa} and so governs the mixing time (i.e. carrier fluid reactant quickly diffuses into the sample stream). Note that this scaling is equivalent to approximating the reactant residence time as approximately equal to a diffusion time of the form s^2/D_{ca}. This time scale, obtained from a simple 1-D model, collapses the experimental data well, especially for low residence times and large flow rates. We also estimate from this analysis that the initial sample stream transverse thickness s (in the transverse y-direction) is 0.1 to 0.2 μm, depending on the sample stream flow rate.

4. Conclusions

Presented was a theta nozzle flow device which provides a novel mix-and-inject architecture compatible with soft X-ray spectroscopy applications. The key theta-capillary component of the system is available commercially. The system was fabricated using standard capillary pulling and laser cutting of simple holders. We also implemented a vacuum line nozzle to catch the liquid jet within 3 cm of the nozzle exits. We used epifluorescence microscopy and fluorescein-iodide quenching experiments to visualize the jets and mixing dynamics. The system produces a single contiguous jet and we observed stable jet lengths of approximately 2 mm across all conditions. The jet velocity was 125 m s^{-1} and had a characteristic diameter of approximately 9 μm. We quantified the degree of mixing as a function of axial position by comparing unquenched with quenched fluorescence image data. For the conditions explored, the sample stream thickness (in the radial direction) was order 0.1 to 0.2 μm for sample flow rates Q_{sa} of 20 to 100 μl min^{-1}. This lamination leads to a best characteristic Lagrangian mixing time of approximately 0.9 μs. The mixing occurs within about 0.5 mm of the nozzle exit. We project that our device will be applicable to windowless X-ray spectroscopy experiments that study fast mixing-triggered chemical reactions in the microsecond time scale. The set-up with a mixing stream that is free flowing on a substrate flow allows the use of high resolution and feature rich L-edge XAS that is sensitive to the electronic and geometric structure of the various states throughout a reaction pathway.

Supplementary material. Supplementary materials are available at https://doi.org/10.1017/flo.2023.15. The data that support the findings of this study are available from the authors.

Declaration of interests. The authors report no conflict of interest.

Funding. The SSRL Structural Molecular Biology Program is supported by the Department of Energy (DOE) Office of Biological and Environmental Research, and by the National Institutes of Health, National Institute of General Medical Sciences (P30GM133894). The contents of this publication are solely the responsibility of the authors and do not necessarily represent the official views of NIGMS or NIH. D.A.H. was supported by a National Science Foundation Graduate Research Fellowship.

Author contributions. D.A.H. and J.G.S. conceptualized the device. D.A.H. fabricated the devices and performed the experiments. A.S.A. developed the diffusion model. All authors analysed mixing data and wrote manuscript.

References

Brändén, G., & Neutze, R. (2021). Advances and challenges in time-resolved macromolecular crystallography. *Science*, *373*, eaba0954.

Crissman, C.J., Mo, M., Chen, Z., Yang, J., Huyke, D.A., Glenzer, S.H., . . . Deponte, D.P. (2022). Sub-micron thick liquid sheets produced by isotropically etched glass nozzles. *Lab on a Chip*, *22*, 1365–1373.

DePonte, D.P., Weierstall, U., Schmidt, K., Warner, J., Starodub, D., Spence, J.C.H., & Doak, R.B. (2008). Gas dynamic virtual nozzle for generation of microscopic droplet streams. *Journal of Physics D: Applied Physics*, *41*, 195505.

Gañán-Calvo, A.M. (1998). Generation of steady liquid microthreads and micron-sized monodisperse sprays in gas streams. *Physical Review Letters*, *80*, 285–288.

Haustein, H.D., Harnik, R.S., & Rohlfs, W. (2017). A simple hydrodynamic model of a laminar free-surface jet in horizontal or vertical flight. *Physics of Fluids*, *29*, 082105.

Henke, B.L., Gullikson, E.M., & Davis, J.C. (1993). X-ray interactions: photoabsorption, scattering, transmission, and reflection at E=50–30000 eV, Z=1–92. *Atomic Data and Nuclear Data Tables*, *54*, 181–342.

Huyke, D.A., Ramachandran, A., Oyarzun, D.I., Kroll, T., DePonte, D.P., & Santiago, J.G. (2020). On the competition between mixing rate and uniformity in a coaxial hydrodynamic focusing mixer. *Analytica Chimica Acta*, *1103*, 1–10.

Huyke, D.A., Ramachandran, A., Ramirez-Neri, O., Guerrero-Cruz, J.A., Gee, L.B., Braun, A., . . . Santiago, J.G. (2021). Millisecond timescale reactions observed via X-ray spectroscopy in a 3D microfabricated fused silica mixer. *Journal of Synchrotron Radiation*, *28*, 1100–1113.

Ishigami, I., Lewis-Ballester, A., Echelmeier, A., Brehm, G., Zatsepin, N.A., Grant, T.D., . . . Rousseau, D.L. (2019). Snapshot of an oxygen intermediate in the catalytic reaction of cytochrome c oxidase. *Proceedings of the National Academy of Sciences of the United States of America*, *116*, 3572–3577.

Knoška, J., Adriano, L., Awel, S., Beyerlein, K.R., Yefanov, O., Oberthuer, D., . . . Heymann, M. (2020). Ultracompact 3D microfluidics for time-resolved structural biology. *Nature Communications*, *11*, 657.

Middleman, S. (1965). Stability of a viscoelastic jet. *Chemical Engineering Science*, *20*, 1037–1040.

Olmos, J.L., Pandey, S., Martin-Garcia, J.M., Calvey, G., Katz, A., Knoska, J., . . . Schmidt, M. (2018). Enzyme intermediates captured "on the fly" by mix-and-inject serial crystallography. *BMC Biology*, *16*, 59.

Plumridge, A., Katz, A.M., Calvey, G.D., Elber, R., Kirmizialtin, S., & Pollack, L. (2018). Revealing the distinct folding phases of an RNA three-helix junction. *Nucleic Acids Research*, *46*, 7354–7365.

Pollack, L., Tate, M.W., Darnton, N.C., Knight, J.B., Gruner, S.M., Eaton, W.A., & Austin, R.H. (1999). Compactness of the denatured state of a fast-folding protein measured by submillisecond small-angle x-ray scattering. *Proceedings of the National Academy of Sciences*, *96*, 10115–10117.

Wang, D., Weierstall, U., Pollack, L., & Spence, J. (2014). Double-focusing mixing jet for XFEL study of chemical kinetics. *Journal of Synchrotron Radiation*, *21*, 1364–1366.

White, F.M. (2006). *Viscous fluid flow* (3rd ed.). New York, NY: McGraw-Hill.

Cite this article: Huyke DA, Avaro AS, Kroll T, Santiago JG (2023). Stream lamination and rapid mixing in a microfluidic jet for X-ray spectroscopy studies. *Flow*, *3*, E25. doi:10.1017/flo.2023.15